New insights into the complex photoluminescence behaviour of titanium white pigments

van Driel, Birgit; Artesani, A.; van den Berg, K.J.; Dik, Joris; Mosca, S.; Rossenaar, B.; Hoekstra, J.; Davies, A.; Nevin, A.; Valentini, G.

DOI
10.1016/j.dyepig.2018.03.012

Publication date
2018

Published in
Dyes and Pigments

Accepted Manuscript

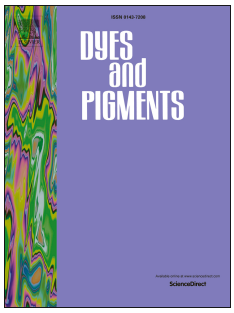

New insights into the complex photoluminescence behaviour of titanium white pigments

Birgit van Driel, Alessia Artesani, Klaas Jan van den Berg, Joris Dik, Sara Mosca, Brenda Rossenaar, Johan Hoekstra, Antony Davies, Austin Nevin, Gianluca Valentini, Daniela Comelli

PII: S0143-7208(17)32546-9

DOI: 10.1016/j.dyepig.2018.03.012

Reference: DYPI 6597

To appear in: *Dyes and Pigments*

Received Date: 21 December 2017

Revised Date: 8 March 2018

Accepted Date: 9 March 2018

Please cite this article as: van Driel B, Artesani A, van den Berg KJ, Dik J, Mosca S, Rossenaar B, Hoekstra J, Davies A, Nevin A, Valentini G, Comelli D, New insights into the complex photoluminescence behaviour of titanium white pigments, *Dyes and Pigments* (2018), doi: 10.1016/j.dyepig.2018.03.012.

New insights into the complex photoluminescence behaviour of titanium white pigments

Birgit van Driel[1,2,3], Alessia Artesani[4], Klaas Jan van den Berg[3], Joris Dik[2], Sara Mosca[4], Brenda Rossenaar[5], Johan Hoekstra[5], Antony Davies[5], Austin Nevin[6], Gianluca Valentini[4], Daniela Comelli[4]

(1) Rijksmuseum Amsterdam, Hobbemastraat 22, 1071 ZC, Amsterdam

(2) Materials for Arts and Archeology, 3ME, TU Delft, Mekelweg 2, 2628 CD, Delft

(3) Cultural Heritage Agency of the Netherlands, Hobbemastraat 22, 1071 ZC, Amsterdam

(4) Physics Department, Politecnico di Milano, Piazza Leonardo da Vinci, 20133 Milano, Italy

(5) AkzoNobel Chemicals, Expert capability Group – Measurement and analytical Science (ECG-MAS), Zutphenseweg 10, 7418 AJ, Deventer

(6) Istituto di Fotonica e Nanotecnologie - Consiglio Nazionale delle Ricerche, Piazza Leonardo da Vinci, 20133 Milano, Italy

b.van.driel@rijksmuseum.nl

Abstract

This work reports the analysis of the time-resolved photoluminescence behaviour on the nanosecond and microsecond time scale of fourteen historical and contemporary titanium white pigments. The pigments were produced with different production methods and post-production treatments, giving rise to a remarkable variability of titanium dioxide powders and, in some cases, to the formation of a complex surface of the crystal agglomerates. The pigments have been further characterized by Raman spectroscopy, scanning transmission electron microscopy coupled with energy dispersive X-ray spectroscopy and inductively coupled plasma atomic emission spectrometry. Our study provides a clear view of the main features of the photoluminescence (PL) emission of anatase- and rutile-based pigments. For both the polymorphs of titanium dioxide the room-temperature photoluminescence emission is complex and involves different relaxation paths, related to shallow levels close to the conduction bands and mid-gap trap states. The PL behaviour appears to be little affected by post-production treatments such as organic and inorganic coatings. Instead, the presence of niobium impurities in the TiO_2 crystal lattice, as residues of the sulphate synthesis process, induce a remarkable quenching of the visible emission of anatase-based pigments. We confirm that rutile-based and anatase-based pigments are significantly different in terms of photoluminescence behaviour. This clear distinction is a valuable point for non-invasive pigment identification by in-situ photoluminescence spectroscopy. In particular, while many organic binding media emit in the visible region, the near-infrared emission of rutile is specific and can likely be used to identify the pigment in more complex materials as paints. This research paves the way to future studies of the photo-physical properties of titanium white pigments, which is imperative

to understand the risk of degradation induced by the well-known photocatalytic activity of this widely used 20th century pigment.

Keywords: Titanium white pigments, time-resolved photoluminescence spectroscopy, EDX spectroscopy, pigment impurities

Declarations of interest: none.

1. Introduction

Titanium white is a collective term for over 580 grades (in 1985)[1] of titanium dioxide-based pigments, respectively made of the anatase and rutile polymorphs of titanium(IV)oxide (TiO_2) [2]. The semiconductor pigment was introduced onto the market at the beginning of the 20th century and was extensively used by artists, including Picasso, Pollock, and Mondriaan [1, 3, 4]. It is still the most widely used white pigment in a broad range of applications (from artist materials to cosmetics), thanks to its high brightness and hiding power. Titanium dioxide, mainly in its anatase form, is widely employed in applications such as air/water purification, self-cleaning and antibacterial action applications [5-7], thanks to its photocatalytic properties activated by absorption of ultraviolet light. For the same reason, the use of titanium white in artist's painting can be of concern as possible cause of degradation problems, such as paint colour change or chalking [8-10]. Despite this issue, it is important to note that only a limited number of degraded works of art containing titanium white have been documented thusfar, possibly as a consequence of the low speed of the degradation process combined with the relatively short existence of the paintings in question [1, 11, 12].

This research aims to study the distinct photoluminescence (PL) behaviour of anatase- and rutile-based polymorfs of TiO_2 pigments. Furthermore, it aims to investigate the possible correlations between the PL properties and pigment features - such as coatings, the presence of impurities, crystal structure and crystal size, - related to the pigment ore, the production process and post-process treatments.

The earliest titanium white pigments, produced at the beginning of the 20th C., were composite pigments composed of barium sulphate and TiO_2 in the anatase form. Later, pure anatase pigments came onto the market followed by rutile pigments in the 1940s [1, 13]. The production of titanium white pigments can follow two main processes: the sulphate process, developed in the 1920s, and the chloride process, stemming from the 1950s and mostly used for the production of rutile [1, 14, 15]. In the first step of the production, the titanium feedstock is converted to a purified intermediate: $TiOSO_4$ or $TiCl_4$. Subsequently, TiO_2 is formed by heating the obtained intermediate. The crystal structure and particulate size of the final product are determined during the latter process and depends mostly on the calcination temperature [16, 17], with the synthetized product being completely transformed into the rutile phase at high temperatures [17-19]. The chloride process can reduce all impurities to below 10-20 ppm. The only compound usually present in the final material is $AlCl_3$, since it is added as a co-oxidant and cannot be completely removed. In the sulphate process, the use of acids helps to remove all impurities except niobium, which incorporates itself in the crystal structure during calcination, and phosphorus, that remains on the particle surface. The niobium impurity, present as Nb_2O_5, causes a slight colour change. Hence trivalent aluminium is added during calcination to compensate for the fifth electron of niobium [1, 16, 17, 20].

A range of post-production treatments, such as organic and inorganic surface coatings are further available to control the pigment behaviour [1, 14, 21-24]. The most common inorganic coating materials are silica and alumina [17, 20]. Depending on the application, a wide variety of organic treatments, including polyhydric alcohols (or polyols), alkano amines, modified silicone oil or others, can be added at the final production stage [1, 17, 25]. The surface of TiO_2 pigments is thus highly complex [20, 25,

26]. Even for uncoated pigments, impurities or additives accumulate on the pigment surface while the pigments crystalize and grow [17]. All these industrial developments give rise to significant variability of titanium dioxide powders available in the past and on the current market, in terms of crystal structure, surface treatments, and impurities.

The two main (tetragonal) crystal structures of TiO_2, anatase and rutile, are characterized by a band gap of 3.18 eV (390 nm) and 3.02 eV (410 nm), respectively [27, 28], with an indirect bandgap for anatase and a quasi-direct bandgap character for rutile [29, 30]. Indeed, extensive research on the photoluminescence properties of TiO_2 as single crystals, thin films and pure or mixed phase nanopowders has been published to indirectly study TiO_2 photocatalytic activity and surface properties[31-38]. The two stable TiO_2 crystalline forms are characterized by well-separated PL bands, with anatase showing a broad visible PL emission (VIS-PL) and rutile a narrower emission in the near-infrared (NIR-PL) [33, 36]. However, in the literature, there is no clear consensus on the nature of the recombination mechanism processes, and, only recently, researchers have proposed new possible schemes of TiO_2 recombination pathways following above and below bandgap excitation [24]. Conversely, fewer works deal explicitly with the PL properties of titanium white as a pigment [39-41]. As PL spectroscopy is a contactless and non-invasive method to investigate the electronic structure of materials, it is particularly attractive for pictorial material characterization such as pigments [42]. The technique is applied as a sensitive method to detect the presence of luminescent materials in artworks and as a research-based tool, to achieve the photo-physical characterization of a variety of inorganic [43-46] and organic artists materials [47, 48].

In this study, by employing time-resolved photoluminescence spectroscopy (TRPL), we investigate the spectral and lifetime PL properties of fourteen samples of titanium white pigments from different historical and contemporary manufactures, produce by the two different processes and with several post-processing treatments. In view of the limited publications on photoluminescence of TiO_2 pigments, this work is explorative and therefore investigates TiO_2 pigments with an array of varying characteristics. TRPL spectroscopy is supported by an investigation of the material structure and composition with Raman spectroscopy, Scanning Transmission Electron Microscopy coupled with Energy Dispersive X-ray spectroscopy (STEM-EDX) and Inductively Coupled Plasma Atomic Emission Spectrometry (ICP-OES). Raman spectroscopy was used to determine the pigments polymorph structure. The STEM-EDX analysis was aimed to investigate the main elemental composition of pigments and possible inorganic coatings, while ICP-OES was employed to assess impurities present in the bulk samples with a higher level of sensitivity than possibile with EDX analysis.

2. Experimental

2.1. Description of the pigment set

The pigments selected for the present study are described in

Table ***1*** and are a selection of available modern and historical pigments for several applications. The pigments were gathered from contemporary manufacturers (Tronox, Kronos, and Huntsman), archival collections from Winsor&Newton and at the Cultural Heritage Agency of the Netherlands (RCE), as well as from a paint mill in the Netherlands (verfmolen de Kat). The powders from archival collections are historical pigments from several different, sometimes unknown, dates. The anatase reference powder was purchased from Sigma-Aldrich. The rutile reference originated from the former Engelhard Corporation (now part of BASF) and was available from a previous study[1].

The pigment powders were analysed as received for TRPL and Raman spectroscopy, while ICP-OES and STEM-EDX required preliminary sample preparation, described in the materials characterization section.

In the following, the pigments will be referred to by their code listed in Table 1.

Table 1: Selection of pigments and their characteristics.

Code	**Name**	**Description** *Based on previous studies, available information from the manufacturer or in the archival sources.*	**Year/period of synthesis**	**Employed synthesis method according to manufacturer**
A1	Hombitan LW	Uncoated anatase [8, 9, 24, 49]	Contemporary	n/a
A2	Huntsman A-HRF	Organically treated to promote dispersion.	Contemporary	Sulphate process
A3	Huntsman A-PP2	Treated with 2% Al_2O_3	Contemporary	Sulphate

[1] It is noted that the rutile powder purchased at Sigma-Aldrich could not be used as the reference rutile sample since it contains detectable amounts of the anatase polymorph, too.

		and 1% SiO_2 + Polyol.		process
A4	Tiofine	Pigment from Tiofine[2].	Pigment likely post-1989 (based on results in Table 2).	n/a
A5	Winsor&Newton 3557	From the Winsor&Newton archive. Likely used in their paints.	The jar was labelled 1941.	Likely sulphate process (chloride process was not in use in 1941)
A6	RCE9649, "Sikkens kist 9"	Pigment from the Sikkens company[3].	Unknown date, likely pre-1962.	n/a
Aref	Sigma-Aldrich 232033	Chemical grade: pure anatase reference.	Contemporary	n/a
R1	Tronox CR-826	SiO_2[10-20%], $Al(OH)_3$ [0-10%], ZrO_2 [0-2%] [8, 9, 24, 49].	Contemporary	n/a
R2	Huntsman HDCD	Organically treated to promote dispersion	Contemporary	Sulphate process.
R3	De kat	Purchased at Dutch 'verfmolen de kat' in 2011.	Contemporary	n/a
R4	Kronos 2310	Received from AkzoNobel in 2011.	Contemporary	n/a
R5	Kronos CL300	From RCE* reference collection. CL could stand for chloride process. After 1965 (chloride process in Europe), around 1996 (pigment reported in a patent [50]).	n/a	Possibly chloride process due to annotation 'CL'
R6	RCE2766	From RCE* reference collection.	n/a	n/a
Rref	Engelhard Rutile	From a previous study conducted by M.Zandbergen at RCE* and Delft University**. Uncoated rutile reference[4].	Contemporary	n/a

**RCE=Cultural Heritage Agency of the Netherlands*
***Unpublished work*

[2] The Rotterdam Tiofine factory (now called Tronox) was founded in 1960. In 1989 the factory switched from the sulphate process to the chloride process. 'TiofineA20" is mentioned in Talens recipe 1971.
[3] Sikkens is now an AkzoNobel paint brand, but it used to be a separate paint company (until 1962). At the Sassenheim plant of AkzoNobel a Sikkens museum was formed. The pigment collection from this museum was later transferred to the RCE, which is where this powder comes from.
[4] Finding a pure, uncoated rutile reference (outside the nano size range) proved challenging. Several powders were purchased at Sigma but characterization showed they were not appropriate in terms of purity. While 'Engelhard' rutile is unclear in terms of manufacturer or provenance, it is a powder of around 100 nm and without inorganic coating.

1

2.2. Material Characterization

Raman spectroscopy

Raman measurements were performed with a homemade device, based on a 785 nm CW laser source and a spectrometer (Acton SpectraPro2150 Princeton Instruments) coupled to a cooled CCD camera (iDUS DV401A, Andor Technology Ltd.) [51]. The grating (600 grooves/mm) allowed the detection of Raman peaks in the spectral range 130–3000 cm^{-1}, with a spectral resolution close to 10 cm^{-1}. Following data acquisition, spectral calibration was performed with the aid of standards samples. Raman spectra of samples were taken with a micro-probe, based on a 20× objective that allows analysis of a circular spot of 50 μm in diameter at a working distance of ~3 mm. The acquisition time is set at 5 s, and the irradiance on the sample is evaluated at 3200 W/cm^2.

Scanning Transmission Electron Microscopy - Energy Dispersive Spectroscopy *(STEM-EDX)*

The powders were prepared for STEM-EDX by dipping a lacey C coated Cu TEM grid in the powder. After removing excess of powder, the particles were imaged in a JEOL 2010F FEG-TEM equipped with a STEM unit and ThermoNoran EDX detector for elemental mapping. Data analysis using phase deconvolution (based on a multivariate approach locating the areas likely to consist out of the same material) was performed using the NSS software. The spatial resolution of the STEM-EDX is 2 nm. The elemental limit of detection, while dependent of overlapping peaks, matrix and absorption effects, is set at 0.1 at%. Measured values are local and do not relate to the bulk of the material.

Inductively coupled plasma atomic emission spectrometry (ICP-OES)

The samples were digested in duplicate with concentrated nitric acid and hydrofluoric acid in a medium pressure microwave digestion system (Anton Paar Go). The elemental composition of the diluted and undiluted samples was measured by ICP-OES using an Agilent 510-vdv in radial and axial mode. To determine the aluminium and silicon concentration the samples were fused in duplicate with lithium metaborate in an automated fluxer (Claisse TheOx) at 1050°C. The hot flux was poured into 1.6M nitric acid, and the element concentrations were analysed with ICP-OES in radial mode. The elemental limit of detection is element specific and reported in table 5 of the supplementary information. It was calculated based on three times the standard deviation from ten blank samples with the same matrix as the measured sample solution. The detection limit values are subsequently rounded up towards and corrected for dilution and sample preparation.

2.3. Time-resolved photoluminescence spectroscopy

The time-resolved photoluminescence system is based on a pulsed laser and on a fast-gated intensified camera coupled to a spectrometer. The camera is capable of high-speed gating to capture the decay kinetic of photoluminescence emission spectra. Excitation of PL from samples is provided by the third harmonic of a Q-switching Nd:YAG laser, emitting sub-ns pulses at 355 nm (CryLas FTSS 355-50, Crylas GmbH, Berlin, Germany) at a repetition rate of 100 Hz. The laser light is delivered onto the sample (powder were pressed into a sample holder of 2 mm diameter). An optical probe allows the excitation of the PL signal from sample surface in a circular spot of 1 mm in diameter with an average power of 2 mW. PL emission from samples is collected in a back-scattering geometry and focused into the entrance slit of an imaging spectrometer. The spectrometer (Acton Research 2300i, focal length = 300 mm, f/4 aperture) mounts two gratings with 150 l/mm with different blazing. The first grating is blazed at 300 nm and

is used for PL acquisition in the spectral range 380–700 nm (UV grating, in the following). The second grating is blazed 800 nm and is used for PL acquisition in the spectral range 600-900 nm (NIR grating, in the following). The kinetics of the emission is detected by a gated intensified camera (C9546-03, Hamamatsu Photonics, Japan), mounted at the exit port of the spectrometer. The detector features an acquisition gate adjustable from 3 ns to continuous mode. A custom-built trigger unit and a precision delay generator complete the system, which has a temporal jitter close to 200 ps.

The measurement procedure is based on the detection of a sequence of PL gated spectra at different delays with respect to laser pulses. In this work, fast and long emissions were detected by employing different gate widths.

- Fast recombination emission was detected using a gate width of 10 ns and recording the emission decay kinetic for the first 100 ns following excitation and exposition time of 1 s.
- Long-lived emission at the microsecond scale was detected with a gate width of 1 μs and recording the decay kinetic for 50 μs following excitation and exposition time of 30 s.

TRPL results are shown in terms of gated emission spectra - displayed following correction for the instrumental efficiency and normalization at emission maximum - and emission decay kinetic profiles. Decay kinetic profiles were further fitted to a multi-exponential decay model (with a maximum of three components) using a nonlinear least square method [44]. The effective lifetime was then calculated as the average of the lifetimes weighted over the amplitude of each component, as stated by the following

equation: $\tau_{EFF} = \frac{\sum_{i=1}^{3} A_i \tau_i}{\sum_{i=1}^{3} A_i}$, where A_i and τ_i refer to the amplitude and the lifetime of each component of the multi-exponential decay model.

3. Results

3.1. Pigment characterization

Raman measurements confirm the expected crystalline structure of powders (SI part 1), with all powders appearing to be made of one specific crystal structure.

STEM-EDX analysis indicates whether an inorganic coating is present on the pigments and provides information about pigment impurities (Figure 1, Table 2 and part 2 of SI). Al or Si based coatings are easily recognized in the images as a 'fuzzy' material surrounding the pigment (lighter in colour). Furthermore, if a thick coating is present, it is common to find loose coating material as well (R1, R3, R6). The coating tends to surround the aggregates rather than primary particles due to clustering. Pigment A3 has a very thin and irregular coating, not always detectable, but loose coating material has been identified (red circle in the photograph). Next to variability in the coating, some variability in size and shape are noted, with A3 and A5 having relatively small particle sizes while A4 has relatively big particle size. Nevertheless, no statistically accurate statement can be made on the average particle size due to the limited number of TEM micrographs. Considering that they are all pigments, we expect them to be between 100 nm (Hombitan LW) and 200-250 nm (Tronox CR). In fact, this is the optimal size to reach the high opacity of titanium white paints [52].

The identification of an organic coating is less straight forward than the detection of an inorganic coating. Phase deconvolution of STEM-EDX mappings of samples A1, A2, A3, and R2 identifies a second phase (yellow colour, circled in red). Examination of the spectra (SI part 2) suggests TiO_2 for both the yellow and the blue phase. The difference

between the phases is the Ti/O ratio, which possibly indicates a coating. However, the second phase could also be due to the accumulation of impurities on the surface during crystal growth [17]. Furthermore, local EDX analysis does not detect the presence of carbon. This can be either because no organic coating is present or because the coating is too thin to generate a signal above the detection limit. Even though the manufacturer of pigments A2, A3 and R2 indicates that an organic coating has been applied, which is assumed in the following, STEM-EDX is not suitable to detect it conclusively. For pigment A3, Huntsman reports that the pigment is polyol treated. As this is a very common organic treatment [17], it is assumed for the other Huntsman pigments as well. A pigment with an inorganic coating is generally also organically treated, and this is taken into account when assuming if an organic treatment is present. Similarly, the older pigments are assumed to be untreated [17]. Determining the organic treatment and distinguishing it from process additives such as grinding aids can be challenging.

In order to quantify the elements in the bulk of the material, ICP-OES was used (Table 2 and SI Part 3). All the pigments that proved to have an inorganic coating (A3, A4, R1, R3, R4, R5 and R6) when analysed by STEM-EDX, also showed Al, Si or Zr (coating materials) in the weight percentage range (>0.1%). Thus, while not localized, ICP-OES can indicate the inorganic coating as well. One exception is A5, where silicon is present in the weight percentage range but is an ore impurity. Phosphorus and niobium are also commonly detected in the weight percentage range (P: A1, A2, A3, A4, A5, Aref, R3, R6 Nb: A5, A6, R2). The presence of niobium can thus provide an indication or the production process (Table 2) as niobium cannot be removed during the sulphate synthesis route. Additionally, potassium was also detected in four pigments in this range. A multitude of elements originating from the ore or the production process were detected in trace

concentration such as calcium, chromium, iron, vanadium, magnesium, and others (SI part 3).

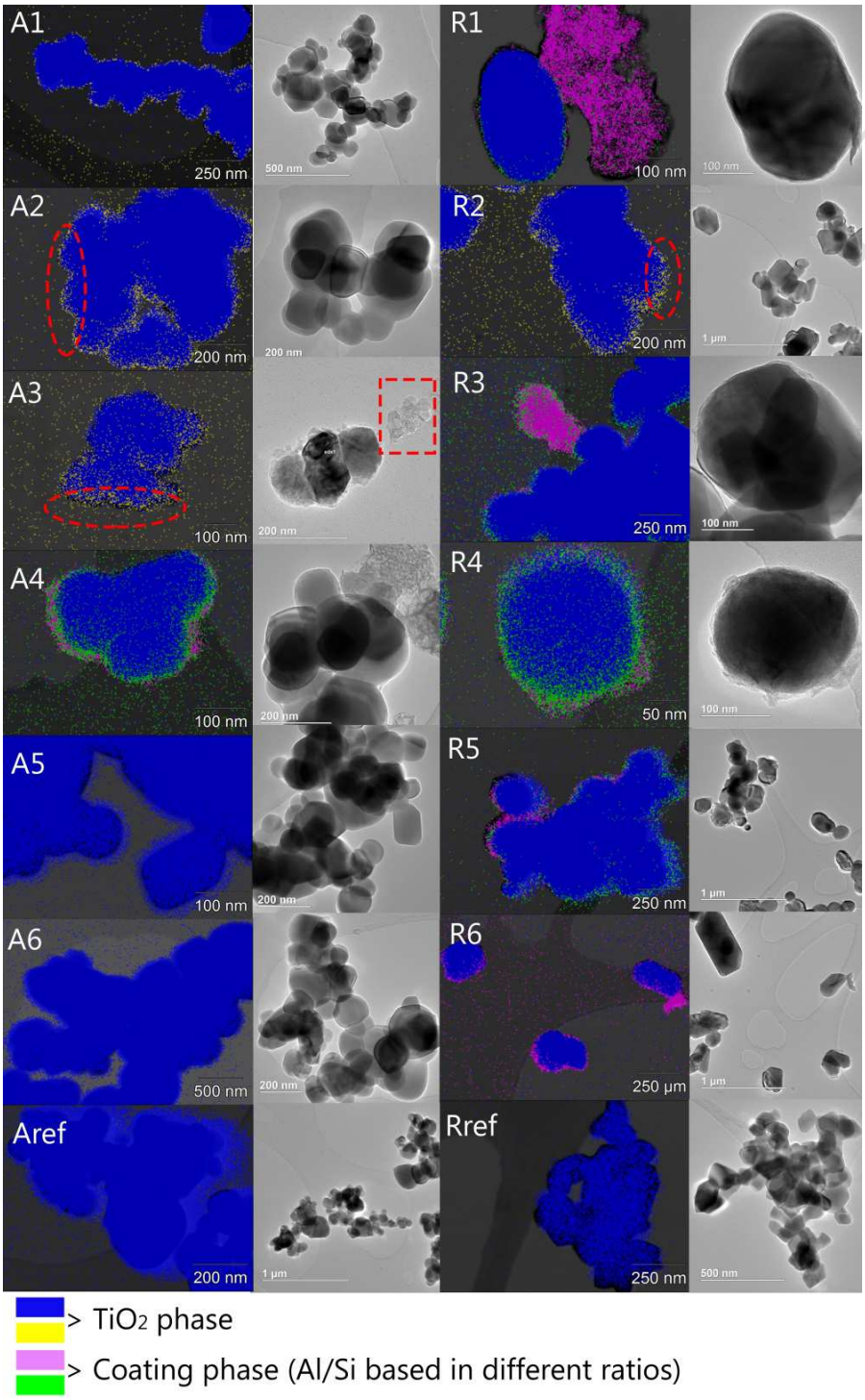

Figure 1: STEM-EDX phase maps and images of the pigments. The phase separation is performed automatically with the NSS software. EDX spectra of the different phases can be found in the supplementary information part 2.

Table 2: Results from ICP-OES (data as received by AkzoNobel presented in SI part 3) and interpretation of the organic, inorganic coating and production process.

Code	Elements >0.1 wt%	Elements in ppm range > 100 mg/kg	Organic coating (based on manufacturer).	Inorganic coating based on STEM-EDX evaluation.	Suggested production process based on elemental composition[5].
A1	K, P	Nb, S, Zr	Unlikely	None	Sulphate process
A2	K, P	Al, Nb, Zr	Likely polyol	None	Sulphate process (confirmation)
A3	Al, P, Si	K, Nb, S, Zr	Likely polyol	Inhomogeneous Al, Si	Sulphate process (confirmation)
A4	Al, P, Si	K, S, Zr	Likely	Inhomogeneous Al, Si	Chloride process[6]
A5	K, Nb, P, Si	Al, Ca, Mg, S, Zn, Zr	Unlikely	None	Sulphate process (confirmation)
A6	Nb	Ca, Fe, K, P, S, Si	Unlikely	None	Sulphate process
Aref	K, P	Nb, Si, Zr	Unlikely	None	Sulphate process
R1	Al, Si	K, P, S, Zr	Likely polyol	Inhomogeneous 2 layers of coating (dense Si + Al)	Chloride process
R2	K, Nb	Al, Ca, P, S, Si, Zr	Likely polyol	No	Sulphate process (confirmation)
R3	Al, P, Zr	Si	Likely	Inhomogeneous Al, Zr coating	Chloride process
R4	Al, Si, Zr	P, S	Likely	Inhomogeneous Al, Si, Zr coating	Chloride process
R5	Al	P, S, Si	Likely	Inhomogeneous Al, Si coating	Chloride process (confirmation)
R6	Al, P, Si	Ca, Nb, S, Zr	Likely	Thick Al, Si coating	Sulphate process
Rref[7]	-	Al, Si	Unlikely	Uncoated (some CuS particles)	Chloride process

[5] The presence/absence of niobium is used as a marker for the production process since niobium cannot be removed in the sulphate process.

[6] A4 is produced by Tiofine (now Tronox), a production facility that switched to the chloride process in 1989. Thus dating the pigment after 1989.

[7] Rref is chosen as a reference because the Sigma-Aldrich rutile was not suitable (see footnote 1 and 4). Raman indicated only the rutile phase. Furthermore, ICP-OES indicated that no impurities are detected in major amounts (>0.1 wt%) and STEM-EDX confirms the absence of an inorganic coating thus confirming the powder is a suitable reference.

3.2. TRPL

Since anatase and rutile-based pigments have different photoluminescence emissions, the TRPL results on the analysed pigments will be discussed separately in the following sections.

TRPL of anatase-based pigments

Figure 2 displays the photoluminescence emission of all the anatase pigments as gated spectra in three different temporal ranges following pulsed excitation. In the first 10 ns after excitation, PL spectra for all samples are characterized by an identical broad emission centred in the green at 500 nm (2.48 eV) (G-PL) with a full width at half-maximum (FWHM) of about 150 nm (0.68 eV). The shape is asymmetric due to the presence of a shoulder in the red, in the following quoted R-PL. At longer delays (time space between 50 and 100 ns after excitation), the R-PL emission appears as the main emitting band in samples A5 and A6, giving rise to a red-shifted emission centered around 630 nm (1.97 eV). In all the other samples it still appears as a slight shoulder of the main G-PL emission. Finally, at microsecond delays (0.2-10.2 μs) in at least two samples (A3 and Aref), it is possible to infer the presence of a faint, but detectable near-infrared emission (NIR-PL) centered in the spectral range 800-850 nm.

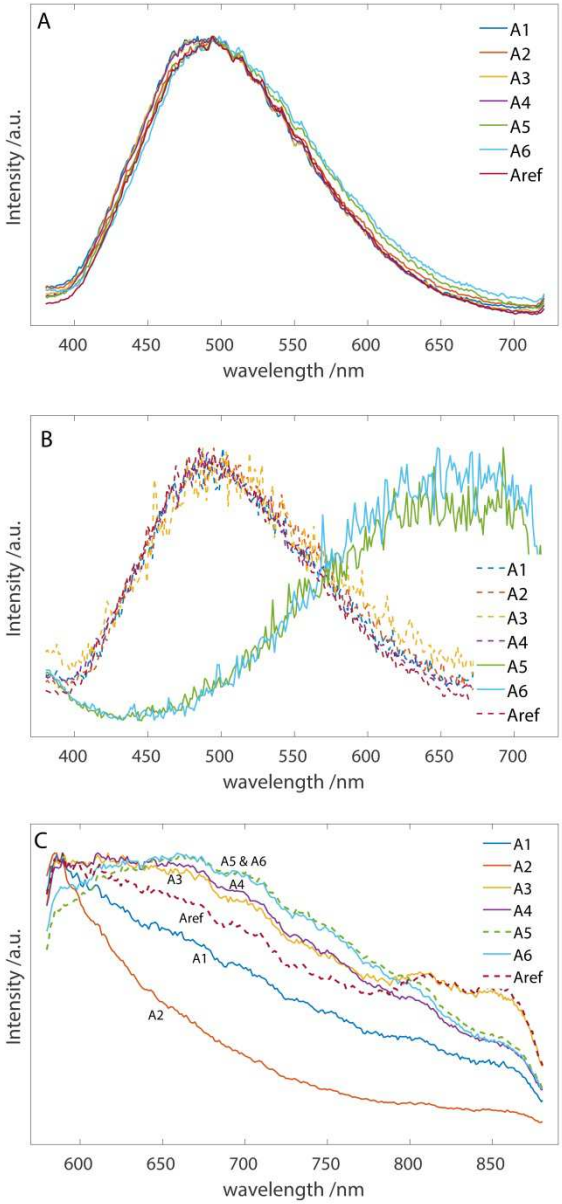

Figure 2: Gated spectrum of anatase pigments in the temporal intervals 0-10 ns(A), 50-100 ns (B) and (C) 0.2-10.2μs after pulsed excitation.

Analysis of the decay kinetics of the bright G-PL emission, Figure 3, indicates that the emission occurs at the nanosecond timescale. The effective lifetime is in the range 3.6-5.2 ns (μ= 4.3 ns, 1σ= 0.6 ns) for all anatase pigments except for samples A5 and A6, which have a more rapid decay and an effective lifetime around 1.8 ns (Table 3).

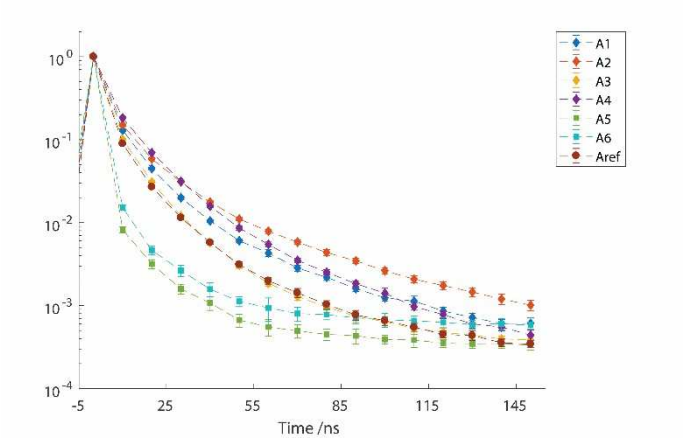

Figure 3: Emission decay kinetic of the G-PL emission (480-520 nm) of anatase pigments.

Table 3: Results of decay kinetics analysis of the G-PL emission of anatase samples (full results presented in SI Part 4, table 6).

Sample	τ (ns) VIS-PL (450-550 nm) -> A
A1	4.3
A2	4.7
A3	3.8
A4	5.2
A5	1.6
A6	2.1
ARef	3.6

TRPL rutile-based pigments

All rutile-based samples show a well-detectable emission at both the nanosecond and microsecond timescales.

In Figure 4A, we report the spectral shape of the signal detected for all samples considering photons emitted in the first 10 ns after pulsed excitation. The gated spectrum appears as the left part of an emission centered at wavelengths minor than 420 nm (or equivalently at energies higher than 2.95 eV), in the following quoted as B-PL. Considering the spectral shape of the emission, it is possible to suggest the presence of two main bands; one peaked at 430 nm (2.88 eV) and the other at 470 nm (2.64 eV).

The emission shape in rutile samples is differentiated by the relative intensity between these two components: the more intense is the second component, the broader is the PL band. Here, we report that samples R1 and Rref are the ones characterized by the narrower PL spectral shape. Analysis of the emission decay kinetic of the B-PL band (Figure 4B) reveals that five pigments are characterized by an effective lifetime in the range 1.8 – 2.8 ns (μ = 2.3 ns, 1σ = 0.4 ns). On the other hand, in samples R2, R6 and Rref the decay kinetic is dominated by a single subnanosecond component with a lifetime close to 0.5 ns (Table 4).

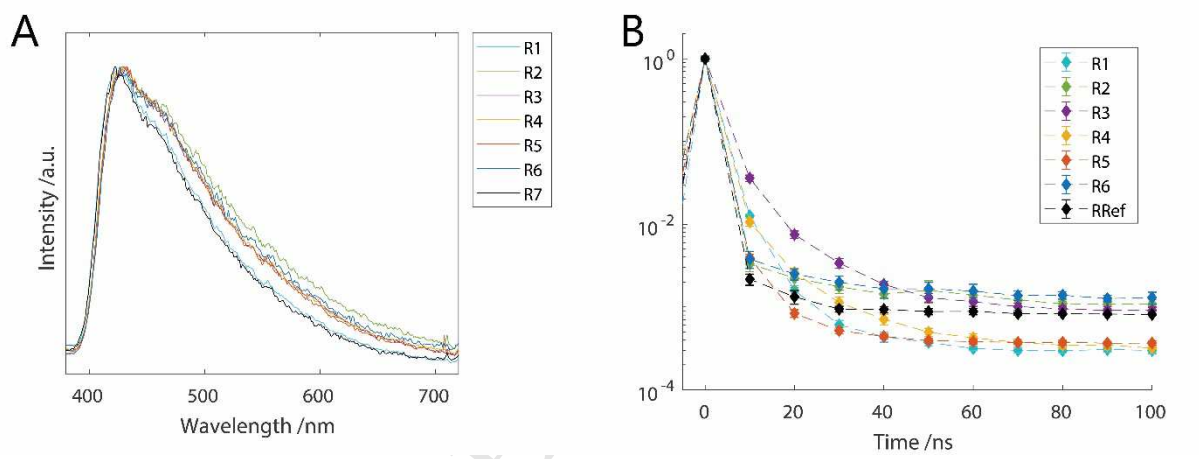

Figure 4: (A) 0-10 ns gated spectrum (normalize) and (B) nanosecond emission decay kinetic in the spectral band (400-550 nm) of rutile pigments

Figure 5A displays the gated spectra detected in the temporal interval between 0.2 and 10.2 μs. In this timespace, all samples have a pretty similar emission shape consisting of a well-defined emission centred around 850 nm (1.45 eV), in the following quoted as NIR-PL. The emission occurs on the microsecond timescale. Following the analysis of the decay kinetic in the spectral band 800-850 nm, Figure 5B, we observe that all rutile-based samples are characterized by an effective lifetime in the range 1.0 -2.4 μs (μ= 1.4 μs, 1σ= 0.6 μs).

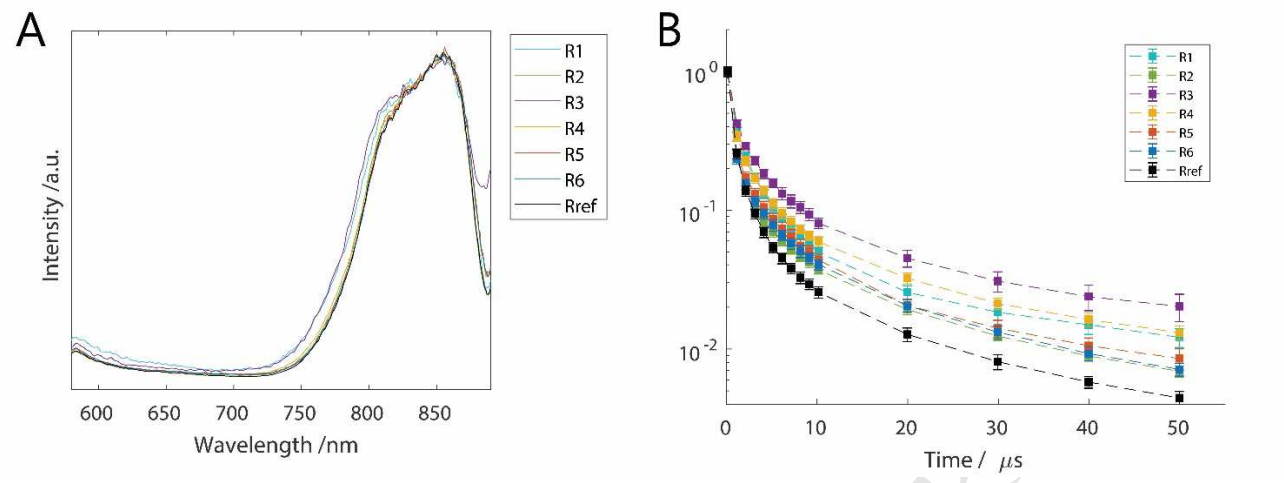

Figure 5: (A) 0.2-10.2 μs gated spectrum (normalize) and (B) microsecond emission decay kinetic in the spectral band (800-850 nm) of rutile pigments.

Table 4: Results of decay kinetics analysis of the two main emissions detected in rutile samples (full results presented in SI Part 4, Table 7 and 8).

Sample	τ (ns) VIS-PL (420-440 nm)	τ (μs) NIR-PL (800-820 nm)
R1	2.2	1.9
R2	0.5	1.0
R3	2.8	2.4
R4	2.3	1.7
R5	1.8	1.0
R6	0.5	0.9
Rref	0.5	1.0

4. Discussion

Material characterization of the available titanium white pigments, made through STEM-EDX, ICP-OES, and Raman, provided a clear distinction regarding crystal structure, inorganic coating and impurities. The organic coating identification instead was less precise and, to better understand it, additional methods should be employed, such as Py-GC-MS. Our selection of pigments is well balanced for an explorative study, with pigments of both crystal types, both production processes and with different types of coatings.

Firstly, TRPL results indicate significant differences between rutile and anatase pigments. This clear distinction is a valuable point for non-invasive pigment identification. In particular, while many organic binding media emit in the visible region [47], the emission for rutile is quite specific and can thus likely be used to identify the pigment in more complex materials such as paints.

Secondly, despite the high variety of available anatase samples, characterized by different inorganic and organic coatings and levels of impurities, the main features of the PL emission vary little among samples. Anatase-based pigments are all characterized by a broad visible photoluminescence emission, centred in the green region (Figure 2). This is in very good agreement with literature data [36, 38, 53, 54], where a PL emission centred between 2.3-2.5 eV (495-540 nm) with a FWHM of 0.9 eV (about 140 nm) is reported. The mechanism behind this radiative recombination is attributed to different kinds of species, without general consensus, such as self-trapped excitons, oxygen vacancies, and defect sites, impurities or reduced metal ions [33]. It is also reported that two distinct components contribute to this visible emission: one centred in the green (G-

PL) and the other in the red (R-PL) [36], as we have detected in all our samples. The most recent research suggests that these two emissions are caused by different recombination mechanisms and are differently influenced by the interaction with molecular oxygen. The G-PL is proposed as the result of radiative recombination of excited electrons in the conduction band with trapped holes. In an O_2 environment, these hot excited carriers are scavenged by chemisorbed O_2, giving rise to the formation of superoxide species and a net decrease of the G-PL emission. On the other hand, the R-PL emission, less sensitive to electrons scavenging, is suggested to be correlated with the recombination of trapped electrons with valence band holes [36, 53]. In our study, we have observed that in the two oldest pigments (A5 and A6), produced by the sulphate process and with no inorganic coating, the relative intensity of the R-PL emission with respect to the G-PL emission, is more relevant than in the other anatase pigments. The shorter emission lifetime of the G-PL band detected in these two samples suggests that light quenching is the main mechanism ruling this intensity variation. Both uncoated, historical samples contain high levels of niobium, and we speculate that these impurities could be responsible for the observed G-PL quenching, but other impurities, like Fe, could be involved as well (see SI, Tables 1, 2 and 5). Indeed, it is recognised that impurities may affect the PL emission behaviour of titanium dioxide [55]. Moreover, considering that samples A5 and A6 are historical, we may expect that the surface of these early synthetized titanium dioxide pigments have not been treated, whereas the opposite is expected for contemporary pigments even when manufacturers do not report it. The non-treated surface of these uncoated pigments could render them more interactive with environmental molecular oxygen, hence promoting the quenching of G-PL emission [36].

Further, in at least two of the analysed samples produced with modern synthesis processes, we detect a NIR-PL emission with spectral and lifetime features that closely resembles the typical PL emission of rutile, as will be further detailed in the next paragraphs. This occurrence suggests that trace amount of the rutile phase can be present in anatase pigments as a consequence of non-perfectly controlled synthesis processes. Here, the use of photoluminescence spectroscopy appears to be ideally suited to detect trace rutile present in concentrations below the detection limit of Raman spectroscopy.

All the rutile pigments analysed in this study are characterized by two distinct emissions. The first is a broad emission in the blue region (B-PL), rarely reported in the literature [56, 57]. The second is a NIR-PL band with a maximum at 850 nm commonly reported for rutile titanium dioxide [1, 36]. The energy position of the NIR-PL emission (about 1.45 eV) with respect to rutile bandgap (3.02 eV) suggest that a deep mid-gap state of unknown chemical origin is necessarily involved. Nowadays, the most reasonable theory for explaining the mechanisms for the NIR emission, as well as its intensity enhancement in an O_2 environment involves the recombination between a mid-gap trapped electron and a free (valence band) hole [38]. Interestingly, Allen et al. reported the detection of two NIR emissions for rutile pigments, one at 830 nm and one at 1015 nm, which, according to the author, should be characteristic for chloride or sulphate processed pigments [39]. As our detector is not sensitive at wavelengths higher than 900 nm, this could not be evaluated in the present research.

Concerning the detected B-PL emission of rutile, whereas the comprehension of the mechanisms behind its de-excitation process is still far to be understood, it is interesting to note that its nanosecond decay kinetic is severely shortened in three of the seven

rutile-based samples giving rise to a sub-nanosecond mono-exponential temporal profile. Two of these samples (R2 and R6) are the only pigments being produced with the sulphate process, and hence containing detectable amounts of niobium, which could act as quenchers of the B-PL emission in rutile samples, too. Instead, no clear explanation can be retrieved for the sub-nanosecond lifetime detected in the Rref sample. Interestingly, the presence of niobium does not affect the spectral shape or the emission lifetime of rutile NIR-PL emission, which is instead affected by other features of the analysed pigment particles with no clear trends on the basis of the present experiments.

In general, it is clear that, whereas the spectral PL features of anatase- and rutile- based pigments are little affected by the complexity and high variety of the selected pigments (mainly with reference to the presence of impurities and coatings), the use of a time-resolved approach allows to probe the sensitivity of the emission lifetime to the micro-environment of excited carriers. This sensitivity gives rise to the detection of different emission decay profiles, which are influenced by many competing factors. On the basis of this research, it is not possible to derive a clear correlation between the emission lifetime and specific properties of titanium white pigment particles – a part for the reported emission quenching induced by niobium impurities.

Similarly, while it is tempting to try to find a correlation between PL properties and the pigment photocatalytic activity, this relation is ambiguous and from our findings, there is no apparent correlation between the luminescence behaviour of the pigments and the presence of inorganic pigment coatings, which are known to strongly influences photocatalytic activity [24]. While others have attempted to correlate chemical properties such as photocatalytic activity with PL intensity [34-36], it is recognised that

the intensity of the emission may be a poor parameter in the analysis of these white pigments, as intensity may depend on many factors including particle size, coating, milling, and heating.

5. Conclusion

The present study highlights the PL properties of several TiO_2 pigments ranging from historical to contemporary and used in different end applications. The most important findings are first that the PL spectral and decay kinetic properties can be influenced by the presence of specific impurities, niobium in particular which is a trace impurity of sulphate processed pigments. Secondly, rutile pigments present a blue emission that has rarely been reported in the literature and that, at present, is not clearly attributed. Furthermore, the study indicates that, due to the well-known and distinct photoluminescence behaviour of rutile and anatase, trace amounts of rutile can be detected in mixtures, while raman spectroscopy fails to detect them.

Our results mostly agree with the previous studies regarding general emission shape, but the increased complexity for pigments compared to nanoparticles and single crystals is evident, which makes the study of luminescence intensity particularly challenging. Further in-depth investigations are worthwhile on well-controlled materials stemming from an identical parent powder. Cryogenic temperatures could allow potentially allow the assessment of luminescence and the influence of processing on luminescence lifetimes at different wavelengths, including those in the IR. In addition to being an explorative step for in depth photoluminescence studies on complex titanium-based pigments, the study also marks the starting point for photoluminescence studies towards titanium white containing paints.

Acknowledgements

This work has received funding from the European Union Horizon 2020 research and innovation programme under grant agreement No. 654148 Laserlab-Europe. Furthermore, the Rijksmuseum is acknowledged for hosting and organizing van Driel's Ph.D. research. AkzoNobel is acknowledged for funding van Driel's Ph.D., as well as for their analytical support. AkzoNobel, Winsor & Newton, the RCE reference collection, Huntsman, Tronox and Sachtleben chemie are acknowledged for providing pigments.

Bibliography

1. Laver M. Titanium White. In: West FitzHugh E, editor. Artists' Pigments: A Handbook of their History and Characteristics, Vol. 3. National gallery of Art, Washington. Londen:Archetype Publications. 1997. 3: 295-355.
2. Eastaugh N, Walsh V, Chaplin T and Sidall R. Pigment compendium, a dictionary and optical microscopy historical pigments, Butterworth-Heinemann. 2004, Burlington: Elsevier.
3. Martins A, Albertson C, McGlinchey C, Dik J. Piet Mondrian's Broadway Boogie Woogie: non-invasive analysis using macro X-Ray fluorescence mapping (MA-XRF) and multivariate curve resolution-alternating least square (MCR-ALS). Herit Sci. 2016; 4.
4. van den Berg KJ, Miliani C, Aldrovandi A, Brunetti BG, de Groot S, Kahrim K, et al. The chemistry of Mondrian's paints in Vicotory Boogie Woogie. In: van Bommel MR, Janssen H, Spronk R, editors. Inside Out Victory Boogie Woogie. Haags Gemeentemuseum, Amsterdam University Press.
5. Benedix R, Dehn F, Quaas J and Orgass M. Application of titanium dioxide photocatalysis to create self-cleaning building materials. 2000; p.157-168
6. Gunnarsson SG. Self-Cleaning Paint: Introduction of photocatalytic particles into a paint system. PhD thesis DTU. 2011.
7. Muneer M, Philip R and Das S. Photocatalytic degradation of waste water pollutants. Titanium dioxidemediated oxidation of a textile dye, Acid Blue 40. Res Chem Intermediat. 1997; 23(3): p. 233-246.
8. van Driel BA, Wezendonk TA, van den Berg KJ, Kooyman PJ, Gascon J and Dik J. Determination of early warning signs for photocatalytic degradation of titanium white oil paints by means of surface analysis. Spectrochim Acta A. 2017; 172: 100-108.
9. Morsch S, van Driel BA, van den Berg KJ and Dik J. Investigating the Photocatalytic Degradation of Oil Paint using ATR-IR and AFM-IR. ACS Appl Mater Interfaces. 2017; 9(11): 10169-10179.
10. Völz HG, Kaempf G, Fitzky HG, Klaeren A. The Chemical Nature of Chalking in the Presence of Titanium Dioxide Pigments. ACS Photodegrad Photostabil Coat. 1981; 151: 163-182.
11. Lauridsen CB, Sanyova J, Simonsen KP. "Analytical study of modern paint layers on metal knight shields: The use and effect of Titanium white. Spectrochim Acta A. 2014; 124: 638-645.
12. Thorn A. Titanium dioxide: a catalyst for deterioration mechanisms in the third millennium." Stud. Conserv. 2000; 45(Supplement-1): 195-199.
13. Stieg FB. Opaque White Pigments in Coatings. ACS Appl Polym Sc. 1985; 285: 1249-1269.
14. de Keijzer M. The history of modern synthetic inorganic and organic artists' pigments. In: Contributions to conservation at the Netherlands Institute for Cultural Heritage, James & James (Science Publishers) Ltd. 2002
15. Phenix A, van den Berg KJ, Soldano A, van Driel BA. The Might of White: formulations of titanium dioxide-based oil paints as evidenced in archives of two artists' colourmen mid-twentieh century. In: ICOM-CC Triennial conference 2017, Copenhagen. 2017.
16. Gazquez MJ, Bolivar JP, Garcia-Tenorio, R and Vaca Federico. A review of the production cycle of titanium dioxide pigment. Mater Sci Appl. 2014.
17. Braun JH, Baidins A, Marganski RE. TiO2 pigment technology: a review. Prog Org Coat. 1992; 20(2): 105-138.
18. Chen YF, Lee CY, Yeng MY and Chiu HT. The effect of calcination temperature on the crystallinity of TiO2 nanopowders. J Cryst Growth. 2003; 247(3): 363-370.
19. Tian C. Calcination intensity on rutile white pigment production via short sulfate process. Dyes pigments. 2016; 133(Supplement C): 60-64.
20. Johansson LS. "Analysing coated powders with XPS." Surf Interface Anal. 1991; 17(9): 663-668.1991
21. Werner AJ. Titanium dioxide pigment coated with silica and alumina. Google Patents. 1969
22. Jacobson HW. Light-stable titanium dioxide pigment composition. Google Patents. 1980
23. Albert D, et al. Titanium dioxide of improved chalk resistance. Google Patents. 1972
24. van Driel BA, Kooyman PJ, van den Berg KJ, Schmidt-Ott A, Dik J. A quick assessment of the photocatalytic activity of TiO2 pigments — From lab to conservation studio! Microchem J. 2016; 126: 162-171.
25. Day RE and Egerton TA. Surface studies of TiO2 pigment with especial reference to the role of coatings. Colloid Surface. 1971; 23(1–2): 137-155.
26. Farrokhpay S. A review of polymeric dispersant stabilisation of titania pigment. Adv Colloid and Interfac. 2009; 151(1–2): 24-32.

27. Valencia S, Marin JM and Restrepo G. Study of the bandgap of synthesized titanium dioxide nanoparticules using the sol-gel method and a hydrothermal treatment. Open Mater Sci J. 2010; 4(1): 9-14.
28. Chinedu EE and Diola B. Ab-initio Electronic and Structural Properties of Rutile Titanium Dioxide." Jpn J Appl Phys. 2011; 50(10R): 101103.
29. Zhu T and Gao SP. The Stability, Electronic Structure, and Optical Property of TiO2 Polymorphs." J Phys Chem C. 2014; 118(21): 11385-11396.
30. Landmann M, Rauls E and Schmidt WG. The electronic structure and optical response of rutile, anatase and brookite TiO 2." J Phys- Condens Mat. 2012; 24(19): 195503.
31. Yamada Y and Kanemitsu Y. Determination of electron and hole lifetimes of rutile and anatase TiO2 single crystals." Appl Phys Lett. 2012; 101(13): 133907.
32. Dozzi MV, D'Andrea C, Ohtani B, Valentini G and Selli E. Fluorine-Doped TiO2 Materials: Photocatalytic Activity vs Time-Resolved Photoluminescence. J Phys Chem C 2013; 117(48): 25586-25595.
33. Shi J, Wang X, Feng Z, Chen T, Chen J and Li C. Photoluminescence Spectroscopic Studies on TiO2 photocatalyst. In: Anpo M and Kamat PV, editor. Environmentally Benign Photocatalysts: Applications of Titanium Oxide-based Materials. Springer New York. 2010; p. 185-203.
34. Stevanovic A, Buttner M, Zhang Z and Yates JT. Photoluminescence of TiO2: Effect of UV Light and Adsorbed Molecules on Surface Band Structure. J Am Chem Soc. 2012; 134(1): 324-332.
35. Stevanovic A and Yates JT. Electron Hopping through TiO2 Powder: A Study by Photoluminescence Spectroscopy. J Phys Chem C. 2013; 117(46): 24189-24195.
36. Pallotti DK, Passoni L, Maddalena P, Di Fonzo F and Lettieri S. Photoluminescence Mechanisms in Anatase and Rutile TiO2. J Phys Chem C. 2017; 121(16): 9011-9021.
37. Knorr FJ, Zhang D and McHale JL. Influence of TiCl4 Treatment on Surface Defect Photoluminescence in Pure and Mixed-Phase Nanocrystalline TiO2. Langmuir. 2007; 23(17): 8686-8690.
38. Mercado CC, Knorr FJ, McHale JL, Usmani SM, Ichimura AS and Saraf LV. Location of Hole and Electron Traps on Nanocrystalline Anatase TiO2. J Phys Chem C. 2012; 116(19): 10796-10804.
39. Allen NS, Bullen DJ and McKellar JF. Luminescence properties and photo-activity of sulphate-processed rutile (titanium dioxide) pigments in commercial polyethylene. J Mater Sci. 1979; 14(8): 1941-1944.
40. Allen NS, Edge M, Sandoval G, Ortega A, Lieauw CM, Stratton J and McIntyre RB. Interrelationship of spectroscopic properties with the thermal and photochemical behaviour of titanium dioxide pigments in metallocene polyethylene and alkyd based paint films: micron versus nanoparticles." Polym Degrad Stabil. 2002; 76(2): 305-319.
41. Janes R, Edge M, Rigby J, Mourelatou D and Allen NS. The effect of sample treatment and composition on the photoluminescence of anatase pigments." Dyes Pigments. 2001; 48(1): 29-34.
42. Nevin A, Cesaratto A, Bellei S, D'Andrea C, Toniolo L, Valentini G and Comelli D. Time-resolved photoluminescence spectroscopy and imaging: new approaches to the analysis of cultural heritage and its degradation. Sensors. 2014; 14.
43. Gonzalez V, Gourier D, Calligaro T, Toussaint K, Wallez G and Menu M. Revealing the Origin and History of Lead-White Pigments by Their Photoluminescence Properties. Anal Chem. 2017; 89(5): 2909-2918.
44. Artesani A, Gherardi F, Nevin A, Valentini G and Comelli D. A Photoluminescence Study of the Changes Induced in the Zinc White Pigment by Formation of Zinc Complexes. Materials. 2017; 10(4): 340.
45. Artesani A, Bellei S, Capogrosso V, Cesaratto A, Mosca S, Nevin A, Valentini G, Comelli D. Photoluminescence properties of zinc white: an insight into its emission mechanisms through the study of historical artist materials. Appl Phys A 2016; 122(12): 1053.
46. Cesaratto A, D'Andrea C, Nevin A, Valentini G, Tassone F, Alberti R, Frizzi R, Comelli D. Analysis of cadmium-based pigments with time-resolved photoluminescence. Anal Method. 2014; 6(1): 130-138.
47. Borgia I, Fantoni R, Flamini C, Di Palma TM, Giardini GA and Mele A. Luminescence from pigments and resins for oil paintings induced by laser excitation. Appl Surf Sci. 1998; 127: 95-100.
48. Comelli D, Capogrosso V, Orsenigo C and Nevin A. Dual wavelength excitation for the time-resolved photoluminescence imaging of painted ancient Egyptian objects. Her Sci. 2016; 4(1): 21.
49. Van Driel BA, van den Berg KJ, Smout M, Dekker N, Kooyman PJ and Dik J. Investigating the effects of artists' paint formulation on degradation rates of TiO2-based oil paints. Unpublished Research.

50. Rinno H, Hessel F, Alberti K. Process for reducing the microbe count in aqueous multi-phase compositions that contain synthetic resin. 1996. Google Patents.
51. Mosca S, Frizzi T, Pontone M, Alberti R, Bombelli L, Capogrosso V, et al. Identification of pigments in different layers of illuminated manuscripts by X-ray fluorescence mapping and Raman spectroscopy." Microchem. 2016; 124(Supplement C): 775-784.
52. Dupont. Ti-pure titanium dioxide, titanium dioxide for coatings. In: Commercial information booklet Dupont. Accessed from https://www.chemours.com/Titanium_Technologies/es_US/tech_info/literature/Coatings/CO_B_H_65969_Coatings_Brochure.pdf. 20-12-2017.
53. Mercado C, Seeley Z, Bandyopadhyay A, Bose S, McHale JL. Photoluminescence of Dense Nanocrystalline Titanium Dioxide Thin Films: Effect of Doping and Thickness and Relation to Gas Sensing. ACS Appl Mater Interface. 2011; 3(7): 2281-2288.
54. Pallotti DK, Orabona E, Amoruso S, Aruta C, Bruzzese R, Chiarella F, et al. Multi-band photoluminescence in TiO2 nanoparticles-assembled films produced by femtosecond pulsed laser deposition. J Appl Phys. 2013; 114(4): 043503.
55. Janes R, Edge M, Robinson J, Allen NS and Thompso F. Microwave photodielectric and photoconductivity studies of commercial titanium dioxide pigments: the influence of transition metal dopants." J Mater Sci. 1998; 33(12): 3031-3036.
56. Harada N, Masako G, Koji I, Hiroshi S, Noriya I, Hideyuki K and Kazuhiro E. Time-Resolved Luminescence of TiO 2 Powders with Different Crystal Structures. JPN J Appl Phys. 2007; 46(7R): 4170.
57. Fujihara K, Izumi S, Ohno T and Matsumara M. Time-resolved photoluminescence of particulate TiO2 photocatalysts suspended in aqueous solutions. J Photochem Photobiol A: Chem. 2000; 132(1): 99-104.

Highlights

- Rutile and anatase pigments have clearly distinguishable photoluminescence emissions.
- The photoluminescence of TiO_2 pigments appears little affected by surface treatments.
- The complexity of the pigment surface complicates photoluminescence interpretation.
- An uncharacteristic blue emission was noted in rutile pigments.
- The presence of niobium, a common impurity, strongly influences photoluminescence.